ACS OMEGA

http://pubs.acs.org/journal/acsodf

Article

# Hierarchical Porous Catalytic Pyrolysis Char Derived from Oily Sludge for Enhanced Adsorption

Dong Han, Xiaoyu Li,* Zhiqiang Gong, Lanyue Jiang, Zhenbo Wang,* and Peikun Liu

Cite This: *ACS Omega* 2021, 6, 20549−20559

Read Online

ACCESS | Metrics & More | Article Recommendations | Supporting Information

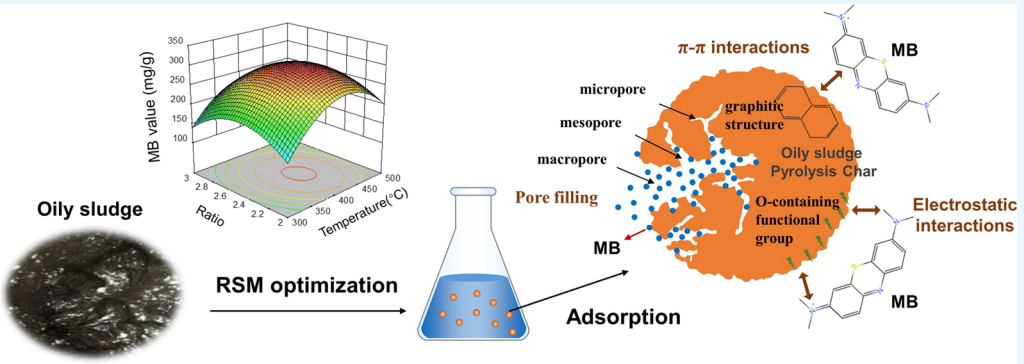


**ABSTRACT:** A novel pyrolysis char (PC), prepared by $H_3PO_4$ catalytic pyrolysis of oily sludge (OS), was presented to remove methylene blue (MB) dye from aqueous solution for the first time. The optimal preparation conditions (catalytic pyrolysis temperature of 411 °C, $H_3PO_4$ impregnation ratio of 2.44, and catalytic pyrolysis time of 59 min) were predicted by the response surface methodology. The optimal PC exhibited favorable hierarchical porous properties, which brought a large adsorption capability (322.89 mg/g). The adsorption process fitted well with the Langmuir model and pseudo-second order model. In addition, thermodynamic parameters showed that the adsorption process was endothermic ($\Delta H^0 > 0$) and spontaneous ($\Delta G^0 < 0$). The adsorption capability was strongly influenced by coexisting metal ions due to the competitive adsorption effect. The inhibition for MB adsorption was arranged in the following order: $Al^{3+} > Fe^{3+} > Mg^{2+} > Ca^{2+} > K^+ > Na^+$. The adsorption mechanism of MB onto the OS-derived PC includes pore filling, $\pi-\pi$ interactions, and electrostatic interactions. The as-obtained PC adsorbent exhibited good reusability performance, which leads to great potential in practical application for wastewater treatment.

## 1. INTRODUCTION

Oily sludge (OS) is a well-known solid waste in petroleum processing during exploitation, transportation, storage, and refining. It poses a great threat to the environment due to the abundant petroleum hydrocarbons and other poisonous metallic elements contained in OS. The proper disposal and sufficient treatment of OS have attracted worldwide attention.[1] Some OS handling techniques have been proposed, such as solvent extraction,[2] ultrasonic irradiation,[3] incineration,[4] stabilization/solidification,[5] biodegradation,[6] and so on. However, the complexity and recalcitrance of the ingredients in OS led a few technologies to reach a compromise between simple operation and low costs.[7]

Incineration of OS in a furnace is the most simple and direct method of utilizing the oil-containing component.[8] However, the toxic burning exhaust would cause secondary pollution.[9] In addition, OS possess a strong coking property when used as fuel. That made OS self-bond and adhere to the inner wall of the firebox, causing serious damage to the furnace. Therefore, it puts forward higher technical requirements for incinerators. Over the years, pyrolysis has shown excellent performance in the waste disposal and resource recovery. OS pyrolysis has also made a great and continuous progress. The main products of OS pyrolysis can be divided into syngas, tar, and char, depending on their different forms. In the initial studies, researchers gave more attention to syngas and tar products in the spirit of oil and gas recovery. The influences of additives or catalysts on pyrolysis oil and gas products have been studied experimentally.[10] However, the pyrolysis char was not given attention until some recent studies showed that pyrolysis chars of OS obtained by some catalytic pyrolysis methods possess favorable physical and chemical properties, which give them a potential for in-depth utilization. The application of OS-based pyrolysis chars in many fields includes adsorption materials for

Received: May 17, 2021
Accepted: July 15, 2021
Published: July 31, 2021

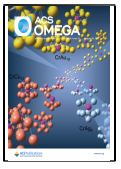

wastewater treatment, electrode materials for supercapacitors,[11] catalysts or catalyst carriers,[12] carbon dioxide storage media,[13,14] and so on. According to the previous works,[15,16] the pyrolysis chars of OS usually have porous structures due to the rapid emission of the syngas from the inside of OS particles. Especially, the decomposition of petroleum hydrocarbons would leave abundant carbonaceous char with a porous structure under proper conditions.

Compared with the expensive commercial products, carbonaceous adsorbents from waste materials are more cost-effective and environmentally friendly.[17] In the past few years, growing interests have been shown in the application of these OS catalytic pyrolysis chars to remove contaminants instead of other adsorbents.[18] In addition, the porous OS catalytic pyrolysis chars usually possess a high specific surface area or abundant functional groups, which are beneficial to adsorption properties for different pollutants, such as phenol,[19] Cr(VI),[20,21] Pb(II), Cd(II),[18] phosphate,[22] dyes,[23] antibiotics,[24] and so on.

Although previous studies have proved the practicability of the carbonaceous adsorbent from OS, the optimization of the preparation process needs to be further studied. The factors affecting structure evolutions and adsorption properties of these adsorbents vary, which make it difficult to optimize the catalytic pyrolysis process reasonability. Extremely tedious work is necessary to run all the tests. In terms of scheme optimization design, the response surface methodology (RSM) has been employed as a statistical approach to evaluate the relationships between independent variables and response variables with fewer experimental trials.[25]

In this work, we described a facile approach to preparing an OS-derived adsorbent. An OS pyrolysis char was obtained under mild conditions with the catalysis of $H_3PO_4$. RSM was applied to find out the optimal route for the preparation of a catalytic pyrolysis char with a 3k Box−Behnken design (BBD). The adsorption capacity of MB dye molecules onto the pyrolysis char was taken as a response value to investigate the effect of three main factors on the synthesis of an OS-based catalytic pyrolysis char (PC), which are catalytic pyrolysis temperature, impregnation ratio of $H_3PO_4$ catalyst, and catalytic pyrolysis time. An optimal synthesis condition for PC to maximize the adsorption capacity was identified by statistical optimization. In addition, PC products synthesized under the optimal conditions possessed an excellent hierarchical porous structure in nature and an MB adsorption amount of 305.51 mg/g, which was competitive in many related studies. The results in this work confirm the possibility of utilization of OS as a precursor of adsorbent for wastewater purification.

## 2. RESULTS AND DISCUSSION

**2.1. Single-Factor Tests.** Single-factor tests were carried out to determine the ranges of independent variables of catalytic pyrolysis temperature, $H_3PO_4$-SC impregnation mass ratio, and pyrolysis time. As shown in Figure 1, the MB adsorption value increased considerably from 141.08 mg/g to 302.69 mg/g with the pyrolysis temperature rising from 300 °C to 400 °C. Nevertheless, the higher temperature (500−700 °C) drove the opposite trend, in which the amounts dropped to 32.49 mg/g gradually. The influence of the $H_3PO_4$-SC impregnation ratio on adsorption performance showed a similar trend to the temperature. The adsorption value increased with the growth of the catalyst impregnation ratio initially until it reached the peak at the best ratio of 2.5 and then decreased. Similarly, time also played an important role during the activation process. The MB adsorption value increased from 219.36 mg/g to 302.69 mg/g, as the heating time extended from 30 min to 60 min. Continuous prolonging of the heating time had no benefit on the MB adsorption value, and the adsorption value fell to 239.56 mg/g at 120 min.

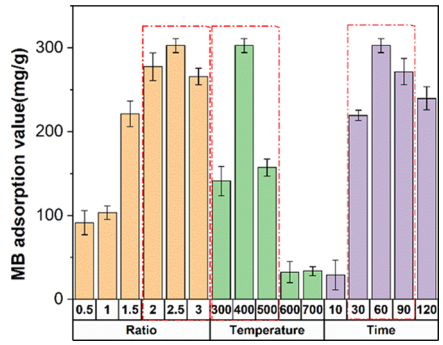


**Figure 1.** Effect of different factors on the MB adsorption capacity.

Generally, adsorption performance always corresponded to the active sites of adsorbents,[26] derived from porous structures and surface functional groups, which requires appropriate preparation conditions according to the above experimental results. The underreaction or overreaction during the preparation of the adsorbents is unfavorable to the formation of the adsorption active structures. Therefore, the appropriate ranges of these three independent variables in the next statistical optimization process were determined as follows: The catalytic pyrolysis temperature is from 300 °C to 500 °C, the $H_3PO_4$-SC impregnation mass ratio is from 2.0 to 3.0, and the catalytic pyrolysis time is from 30 min to 90 min.

**2.2. RSM Tests.** *2.2.1. Establishment of the Statistical Model.* The design of BBD and obtained experimental results are presented in Table 1. The predicted values calculated from the fitting formula are also displayed. It can be observed that MB adsorption values reached the maximum (302.486 ± 3.591

**Table 1. BBD with Three Key Factors and Their Corresponding Experimental and Predictive Values**

| | temperature (°C) | | ratio ($H_3PO_4$:SC) | | time (min) | | adsorption values (mg/g) | |
|---|---|---|---|---|---|---|---|---|
| run | $X_1$ | code | $X_2$ | code | $X_3$ | code | actual | predicted |
| 1 | 400 | 0 | 2 | −1 | 30 | −1 | 204.691 | 205.10 |
| 2 | 300 | −1 | 2.5 | 0 | 90 | 1 | 105.108 | 103.99 |
| 3 | 300 | −1 | 2 | −1 | 60 | 0 | 148.077 | 147.94 |
| 4 | 500 | 1 | 2.5 | 0 | 90 | 1 | 197.098 | 197.39 |
| 5 | 400 | 0 | 2.5 | 0 | 60 | 0 | 306.077 | 302.45 |
| 6 | 400 | 0 | 2.5 | 0 | 60 | 0 | 298.896 | 302.45 |
| 7 | 400 | 0 | 3 | 1 | 30 | −1 | 180.747 | 179.52 |
| 8 | 400 | 0 | 3 | 1 | 90 | 1 | 163.125 | 162.72 |
| 9 | 400 | 0 | 2.5 | 0 | 60 | 0 | 304.162 | 302.45 |
| 10 | 400 | 0 | 2.5 | 0 | 60 | 0 | 304.125 | 302.45 |
| 11 | 300 | −1 | 2.5 | 0 | 30 | −1 | 175.818 | 175.53 |
| 12 | 400 | 0 | 2.5 | 0 | 60 | 0 | 298.981 | 302.45 |
| 13 | 300 | −1 | 3 | 1 | 60 | 0 | 137.034 | 138.56 |
| 14 | 500 | 1 | 2.5 | 0 | 30 | −1 | 155.562 | 156.69 |
| 15 | 400 | 0 | 2 | −1 | 90 | 1 | 189.815 | 191.06 |
| 16 | 500 | 1 | 3 | 1 | 60 | 0 | 158.135 | 158.26 |
| 17 | 500 | 1 | 2 | −1 | 60 | 0 | 204.323 | 202.80 |



https://doi.org/10.1021/acsomega.1c02575
ACS Omega 2021, 6, 20549−20559

mg/g) at the center point: activation temperature of 400 °C, $H_3PO_4$-SC impregnation mass ratio of 2.5, and activation time of 60 min. To find a suitable regression model, a fit summary was prepared at the beginning. The results of sequential model sum of squares, lack-of-fit tests, and model summary statistics are exhibited in Table S2. The lowest *p*-value (<0.0001) in the sequential model sum of squares test meant that the quadratic model was the highest-order polynomial where the additional terms were significant. In addition, the quadratic model had an insignificant lack of fit, which was also expected in the model development.[27] In addition, the quadratic model had the minimum of standard deviation and the maximum $R^2$, $R_{adj}^2$, and $R_{pred}^2$. In summary, the quadratic model was the best option for further study.

*2.2.2. Statistical Analysis.* The accuracy of the selected quadratic model was further evaluated by the analysis of variance (ANOVA). The results of ANOVA are displayed in Table S3, where the value of "Prob>F" less than 0.01 suggested that the quadratic model had a credible level of 99%.[28] The *F*-value of this model was confirmed as 1049.72 and the *p*-value was less than 0.0001. It implied that the quadratic model was significant, and there was only a 0.01% chance that such a large *F*-value could occur due to noise.[29] On the contrary, the *p*-value greater than 0.10 meant that this term was not significant. In this experiment design, all terms were highly significant, except an interactive coefficient of $X_2X_3$. In addition, the "Lack of Fit F-value" of 0.33 implied that the lack of fit was not significant relative to the pure error. In this case, it is not necessary to add more runs to estimate the additional terms for building a higher-order model.

The goodness of fit between the actual response and the predicted response was appraised. Results including several typical parameters are displayed in Table S4. The high determination coefficient of 0.9993 showed the adequacy and validity of regression, which is illustrated in Figure 2 as well.

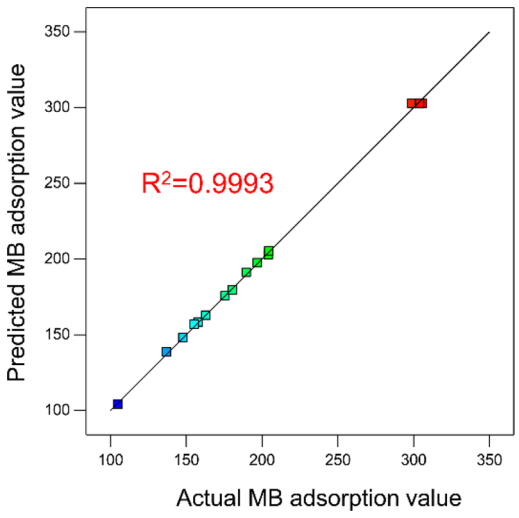


**Figure 2.** Plot of predicted *vs* actual adsorption value of MB.

The "Pred R-Squared" of 0.9967 was in reasonable agreement with the "Adj R-Squared" of 0.9983, in which the difference was ideally less than 0.2 according to a rule of thumb. The coefficient of variation (CV, %) is another statistic to measure the variation of the observed values in the data, in which CV < 10% is desirable. The ratio of adequate precision measures the signal-to-noise ratio. A ratio greater than 4 is preferable. As shown in Table S4, the calculated values of CV and adequate precision were 1.34 and 92.892, respectively, which were far from the threshold values. The results indicated that the established quadratic model was credible and reproducible. Finally, a second-order polynomial equation in terms of codes that fit the experimental data was established as follows:

$$Y = 302.45 + 18.64X_1 - 13.48X_2 - 7.71X_3 - 8.79X_1X_2 + 28.06X_1X_3 - 0.69X_2X_3 - 83.38X_1^2 - 57.18X_2^2 - 60.67X_3^2$$

The equation reveals a correlation between the dye adsorption value and the preparation condition in a mathematical form, where the positive coefficient implies a synergistic influence, and the negative coefficient plays an antagonistic role.[27]

*2.2.3. Interpretation of Residual Diagnosis.* Further, the adequacy of the proposed quadratic model was inspected by the diagnostics node. As illustrated in Figure 3a, the normal probability conformed closely to a straight line, which proved effectively that the residuals obeyed normal distribution. Figure 3b gives the plot of the residuals versus the ascending predicted response values. It verifies the assumption of constant variance. The relationship between residuals and the experimental run order is shown in Figure 3c. It checks for lurking variables that may influence the response. Both plots above show a random scatter without any particular pattern. The residuals drift randomly around the 0 value within a constant range (−3 to +3) of residuals across the graph, and there is no obvious outlier. Thus, the data were independent of each other. The leverage is a measure of how each point influences the model fit. The model will be controlled and goes through the point, which has a leverage of 1.0. As shown in Figure 3d, all the runs expectedly had a leverage less than 1.0. By all the above analyses, the mathematical model established is proved to be reliable and can be used to express the relationship between the independent variables and response.

*2.2.4. Response Surface Analysis.* The 3D surface plots and contours generated by the software are displayed in Figure 4. The plots contributed to investigating the optimum level of each independent variable and the combined effects of these variables on the response. The interactions between two independent variables can be explored by keeping the third factor at a central level. Obviously, as a result of the existence of visible peaks, the optimum levels were all controlled within the range determined in the previous single-factor experiments. Additionally, the optimum conditions for the synthesis process were close to the center point of 400 °C, 60 min, and 2.5:1 for the temperature, activation time, and mass ratio of $H_3PO_4$/SC, respectively. The shapes of the contours can indicate the intensity of interaction between two variables.[30] It is clear that the more elliptical the contours are, the more prominent the interactions are, and vice versa. Therefore, the interactions of temperature−ratio (Figure 4a,b) and temperature−time (Figure 4c,d) were strong. Conversely, Figure 4e,f infers the negligible interaction between ratio and time with a contour closest to the circle. The result was consistent with ANOVA where the term of "BC" (the value of Prob > *F* was 0.6372) was not significant.

*2.2.5. Numerical Optimization.* To determine the optimum conditions of adsorbent preparation for maximizing the MB adsorption capacity, the optimization process based on the


https://doi.org/10.1021/acsomega.1c02575
ACS Omega 2021, 6, 20549−20559

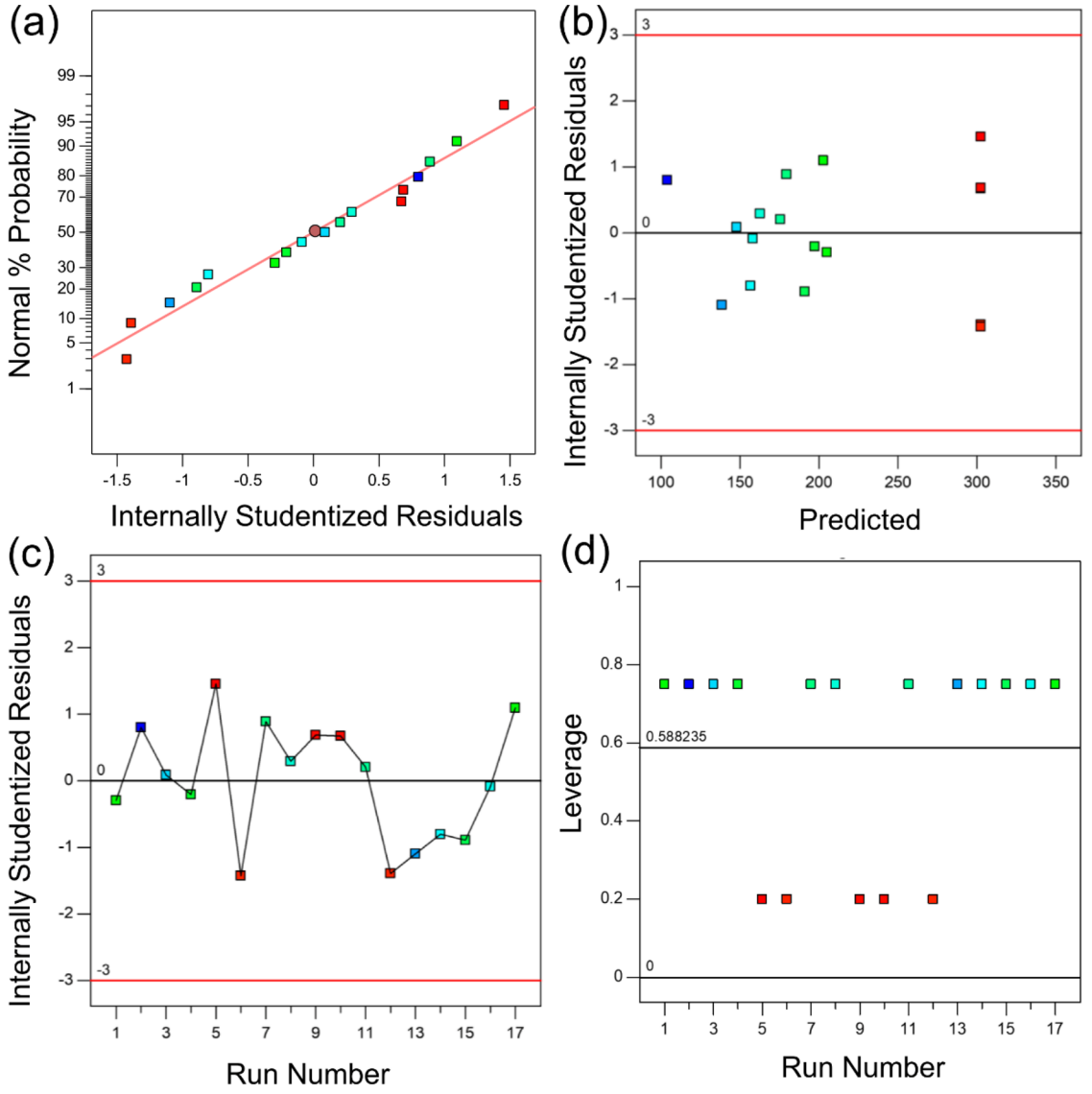


**Figure 3.** Residual diagnostics plot for the model. (a) Normal probability distribution of residuals, (b) plots of residuals *vs* predicted results, (c) relationship between the leverage score and the experimental run order, and (d) residuals displayed in the order of experimental run number.

desirability function was operated by setting the goal values of independent variables "in range" and response "maximize", As illustrated in Figure 5, the desirability score of 0.992 leads to a maximum MB adsorption capacity of 304.487 mg/g when independent variables were set as 411.256 °C for the activation temperature, 2.43704 for the impregnation ratio, and 58.8849 min for the activation time. Subsequently, the validity and accuracy of statistics-optimized conditions were examined by a duplicate test. The MB adsorption value of 305.51 mg/g is guaranteed under the conditions of 411 °C for the temperature, 2.44 for the impregnation ratio, and 59 min for the activation time. The actual value observed from experiments is in high agreement with the predicted value.

**2.3. Characterization of the PC Sample.** According to the results of the above optimal experimental design, the final PC adsorbent was prepared. The structure characteristics of this sample are shown in Figure 6. There are two obvious wide peaks in the XRD pattern (Figure 6a), located at 24.5° (002) and 44.6° (101), which indicate the coexistence of amorphous carbon and a graphite structure in samples, respectively.[31] At the same time, the D band and G band around 1350 and 1600 $cm^{-1}$ in the Raman spectrum are also observed. The ratio of the intensities of these two bands is usually used to estimate the degree of disorder of carbon materials. The $I_D/I_G$ ratio in Figure 6b is close to 1.0, which indicates the highly disordered graphitic structure with defects in the PC material.[32] As we know, this defective structure might mean well-developed pores and abundant surface groups, which are all beneficial to adsorption properties.

To further determine the porosity of PC, a $N_2$ adsorption–desorption test was carried out (Figure 6c). The isotherm displays type IV with an H4 hysteresis loop. In detail, the quantity of $N_2$ adsorption that increased with a nearly vertical slope at lower $P/P_0$ is caused by the micropores in the sample. The broad hysteresis loop ranging from 0.43 to 0.99 of $P/P_0$ is generated by the capillary condensation of $N_2$ inside the mesopores.[33] The specific surface area is calculated as 318.198 $m^2/g$ and the total pore volume of PC is 0.259 $cm^3/g$. Although the surface area is not particularly high, the pore size distribution presents the characteristics of a uniform hierarchical structure, which can promote the adsorption of MB dye. The hierarchical porous structure calculated here is in


https://doi.org/10.1021/acsomega.1c02575
ACS Omega 2021, 6, 20549−20559

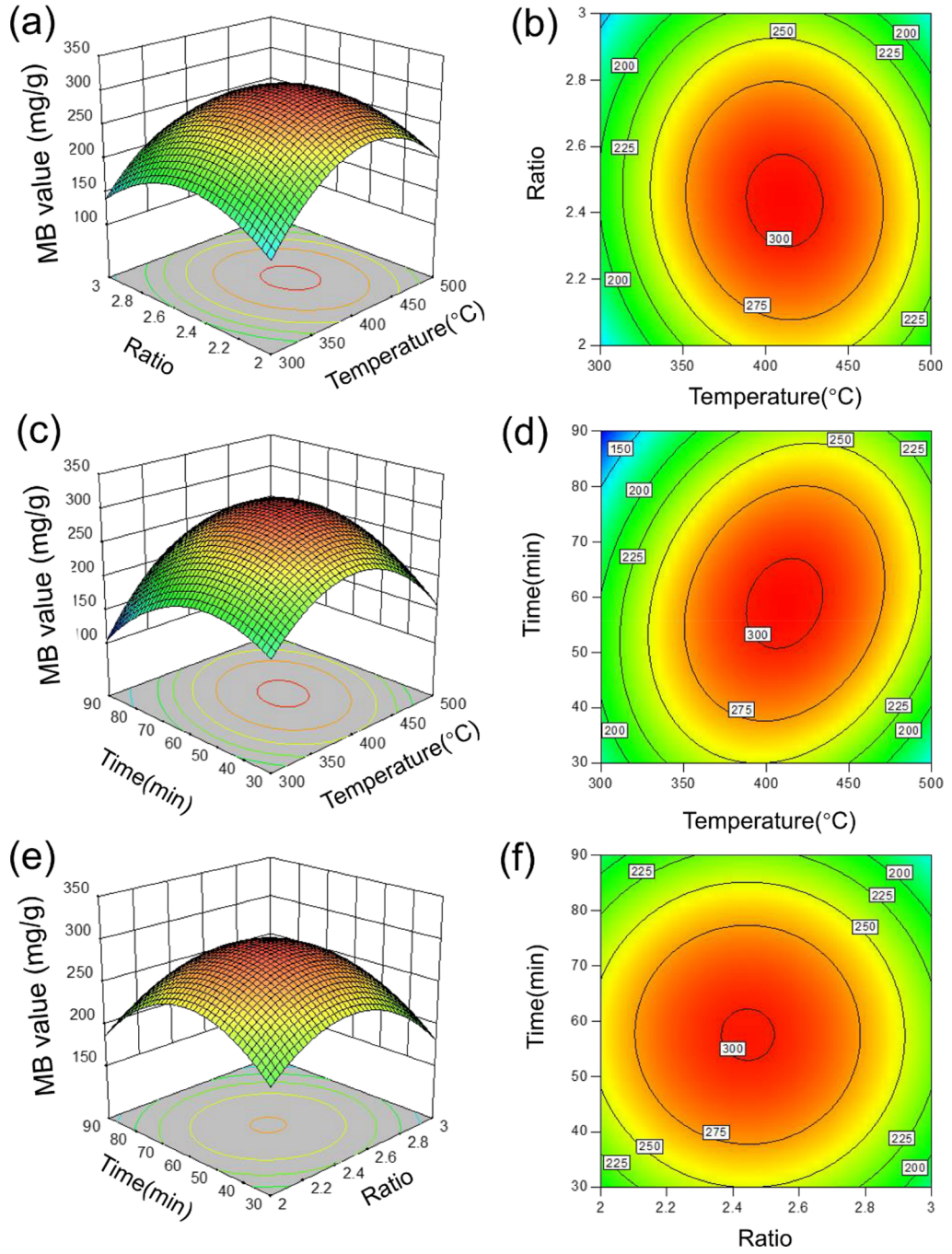


**Figure 4.** (a, c, e) Response surface and (b, d, f) respective contour plots of the model.

good agreement with SEM and TEM images shown in Figure 6e,f. The skeleton of PC materials was severely eroded by acid pickling and catalytic reaction, leaving only a broken fragment and interconnected porous structure, which are favorable for adsorption of dye molecules. XPS analysis was also performed to determine the surface chemical states of the PC material to establish the mechanism of adsorption. As shown in Figure S1, these O-containing functional groups especially hydroxyl and carboxyl groups could generate the electrostatic attraction effect with MB ions, which may promote the adsorption performance of the PC material.

**2.4. Adsorption Experiments.** *2.4.1. Adsorption Isotherm.* The adsorption capacity of the optimal PC toward MB increased with the increase in the initial concentration of dye (Figure 7). This is because of the higher concentration gradient at the solid−liquid interfaces. The mass transfer of MB toward the PC surface could be promoted by the driven force caused by that concentration gradient, which satisfies the generalized Fick Law to some extent.[34] In addition, a higher temperature could also promote the maximum adsorption capability, implying that the adsorption process may be endothermic. It means that the adsorption process has a strong chemical adsorption effect, which prefers a higher temperature.

The fitting results of Langmuir isotherm and Freundlich isotherm models for the MB adsorption are listed in Table 2. It is shown that the Langmuir model got better fitting results ($R^2$ > 0.99). It indicates that the dye molecules were adsorbed by


https://doi.org/10.1021/acsomega.1c02575
ACS Omega 2021, 6, 20549−20559

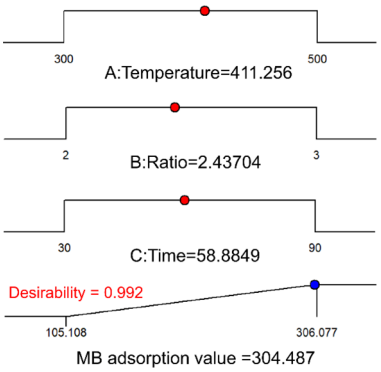


**Figure 5.** Plots of numerical optimization based on the desirability function.

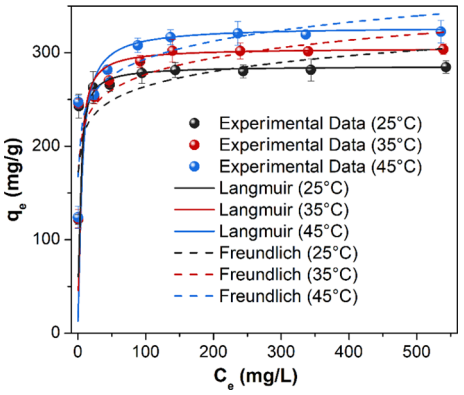


**Figure 7.** Adsorption equilibrium experiment results and isotherm model fitting curves at different temperatures.

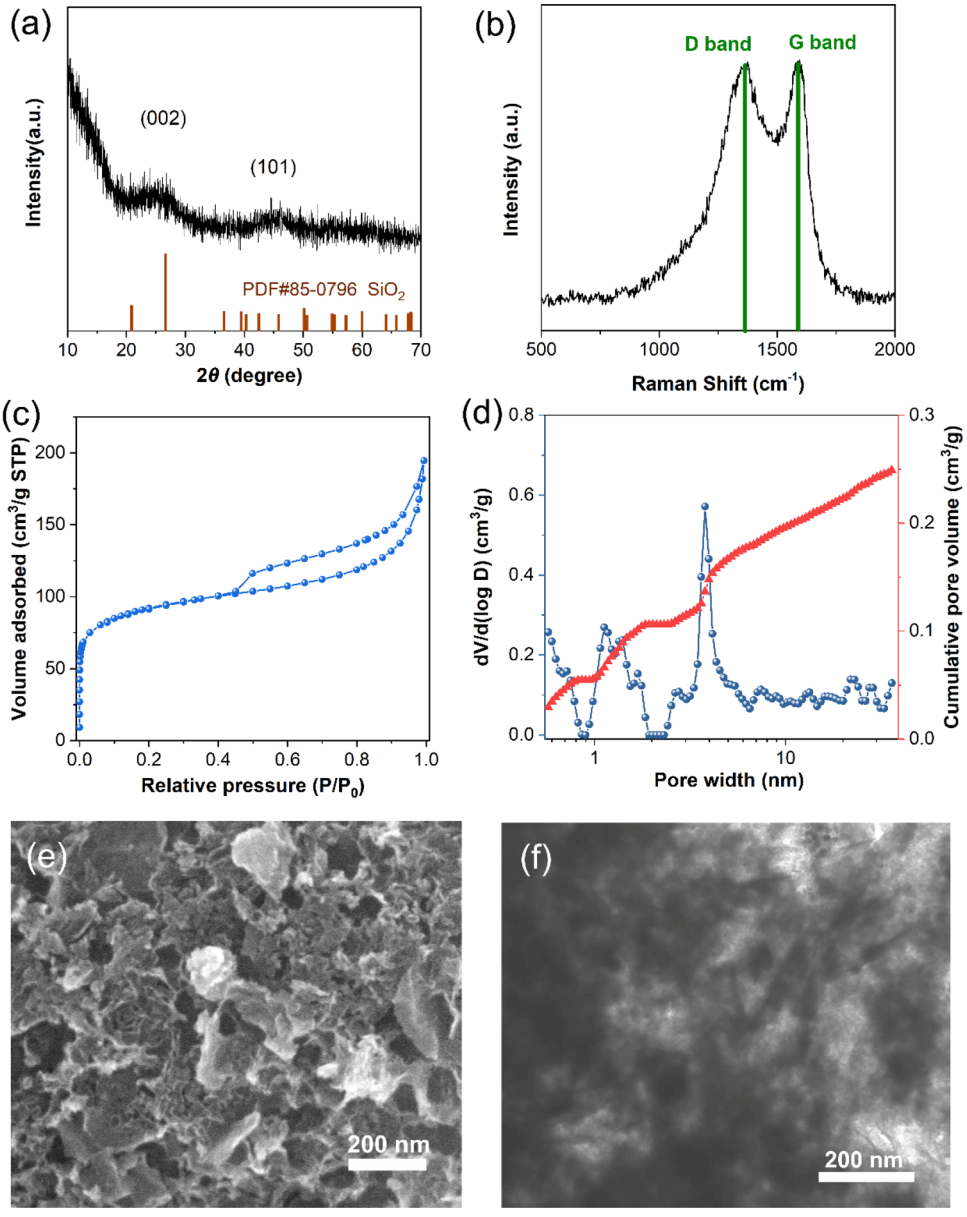


**Figure 6.** (a) XRD pattern, (b) Raman spectrum, (c) $N_2$ adsorption−desorption curve, (d) pore size distribution curves, (e) SEM image, and (f) TEM image of the PC sample obtained under the optimal experimental conditions.



https://doi.org/10.1021/acsomega.1c02575
*ACS Omega* 2021, 6, 20549−20559

**Table 2. Adsorption Isotherm Model Fitting Results and Model Parameters of Isotherm Models**

| temperature (K) | | | 298 | 308 | 318 |
|---|---|---|---|---|---|
| experimental adsorption value $q_{e,exp}$ (mg/g) | | | 282.69 | 305.51 | 322.89 |
| Langmuir isotherm | $q_m$ | (mg/g) | 285.71 | 304.88 | 327.87 |
| | $K_L$ | (L/mg) | 0.4094 | 0.3388 | 0.2032 |
| | $R_L$ | | 0.003−0.789 | 0.003−0.850 | 0.007−0.960 |
| | $R^2$ | | 0.9999 | 0.9999 | 0.9997 |
| Freundlich isotherm | $K_F$ | $(mg/g)(L/mg)^{1/n}$ | 178.95 | 183.06 | 193.37 |
| | $1/n$ | | 0.0844 | 0.0897 | 0.0905 |
| | $R^2$ | | 0.5635 | 0.6255 | 0.7153 |

the monolayer on the homogeneous PC surface, which is an obvious physical adsorption process. Combined with the previous analysis results, the adsorption process of MB onto PC could be identified as a combination of chemical and physical adsorption effects. All the separation factor $R_L$ values fell into 0 to 1 within the concentration range investigated in this experiment.[35] It proves that all the MB adsorption processes are favorable. The maximum adsorption values $q_m$ calculated from the Langmuir model were 285.71, 304.88, and 327.87 mg/g, respectively. These values are higher than the recent reported adsorbents shown in Table S7, which means that the PC material is a promising adsorption material.

*2.4.2. Adsorption Kinetics.* The kinetic investigation was also conducted to determine the rate-limiting factors of this adsorption process. As shown in Figure 8, all plots of $q_t$ *vs* $t$

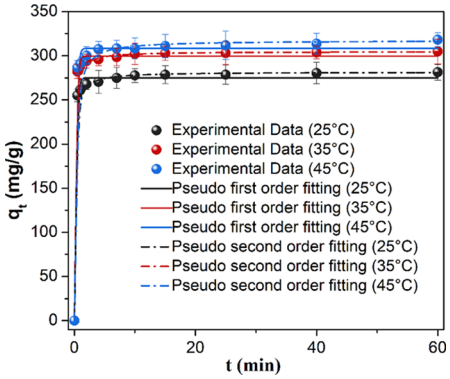


**Figure 8.** Adsorption kinetic experiment results and kinetic model fitting of the adsorption capacity in different temperatures.

exhibit a similar trend, which can be divided into three different stages. First, a linear increase with a steep slope occurs within the first minute. Dye molecules diffuse from the liquid phase to the surface of the liquid film that formed on the surface of PC adsorbents due to hydration and subsequently overcome the resistance of the liquid film to reach the surface of PC.[36] Second, a gradual transition to equilibrium occurs. It may indicate that the dye molecules diffuse from the external surface to the adsorption sites on the internal surface of the PC. Third, the adsorption curves reach a plateau region, which means the adsorption saturated condition.

The fitting parameters of the two kinetic models are listed in Table 3. It is obvious that the pseudo-second-order model fitted better than the pseudo-first-order model with experimental data at each temperature ($R^2 > 0.999$). As is known, the pseudo-second-order kinetic model assumes that the adsorption rate is determined by the square value of the number of adsorbed vacancies on the adsorbent, which plays a vital role in chemical sorption. Therefore, all the above three

**Table 3. Fitting Results and Model Parameters of Kinetic Models**

| temperature (K) | | | 298 | 308 | 318 |
|---|---|---|---|---|---|
| experimental adsorption value $q_{e,exp}$ (mg/g) | | | 282.69 | 305.51 | 322.89 |
| pseudo-first-order model | $q_{e,cal}$ | (mg/g) | 275.03 | 299.62 | 308.34 |
| | $k_1$ | (1/min) | 5.0817 | 5.5723 | 5.1104 |
| | $R^2$ | | 0.9948 | 0.9972 | 0.9941 |
| pseudo-second-order model | $q_{e,cal}$ | (mg/g) | 281.69 | 304.88 | 317.46 |
| | $k_2$ | (g/mg/min) | 0.027 | 0.033 | 0.015 |
| | $R^2$ | | 0.9999 | 0.9999 | 0.9999 |

stages were the rate-limiting step of adsorption as the possibility of affecting the number and activity of adsorption sites.

*2.4.3. Thermodynamics.* The thermodynamic analyses were performed to further understand the adsorption behavior. As shown in Figure 9, the $\Delta H^0$ and $\Delta S^0$ could be obtained from

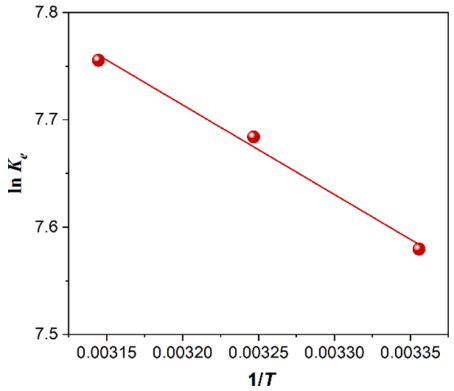


**Figure 9.** Thermodynamic analysis for the adsorption of MB on PC.

the slope and the intercept of the fitting plot of ln $K^0$ *vs* $1/T$. The calculation results are listed in Table 4. The negative values of $\Delta G^0$ suggest that the adsorption process is spontaneous in nature. In addition, the positive values of $\Delta S^0$ mean that the randomness of the adsorption system is increasing, which indicates that the system tends to be more stable. The positive values of $\Delta H^0$ suggest that the process is

**Table 4. Thermodynamic Parameters for the Adsorption of MB onto PC**

| temperature (K) | $\Delta G^0$ (kJ/mol) | $\Delta H^0$ (kJ/mol) | $\Delta S^0$ (kJ $mol^{-1}$ $K^{-1}$) |
|---|---|---|---|
| 298 | −18.779 | 6.950 | 0.086 |
| 308 | −19.698 | | |
| 318 | −20.505 | | |



https://doi.org/10.1021/acsomega.1c02575
ACS Omega 2021, 6, 20549−20559

endothermic, in keeping with the adsorption isotherm and kinetic analyses. From another point of view related to the adsorption mechanism, the increasing temperature causes more adsorption sites of the adsorbent to be exposed by reducing the number of water molecules adsorbed on hydrophilic groups on the adsorbent surface through hydrogen bonding.

*2.4.4. Effects of Coexisting Ions.* Commonly, the presence of other ions in wastewater would affect the adsorption performance of dye pollutants. The MB adsorption experiments of PC were carried out under the coexistence of different cations ($Na^+$, $K^+$, $Ca^{2+}$, $Mg^{2+}$, $Fe^{3+}$, and $Al^{3+}$). As shown in Figure 10, all the adsorbed values with the existence

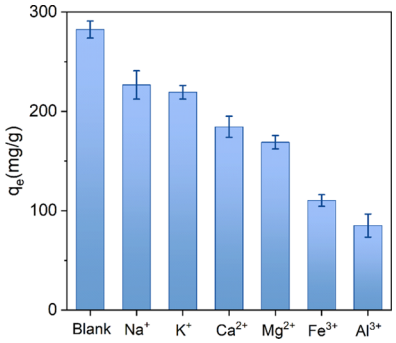


**Figure 10.** Effects of different coexisting cations on MB adsorption onto PC.

of background ions were smaller than the blank group. It indicates that these cations inhibited the adsorption of MB onto PC. The degree of inhibition is arranged in the follow order: $Al^{3+}$ > $Fe^{3+}$ > $Mg^{2+}$ > $Ca^{2+}$ > $K^+$ > $Na^+$. The corresponding adsorption capacities were 85.08, 110.36, 168.93, 184.54, 219.28, and 226.66 mg/g, respectively. The cations with higher valence more strongly inhibited MB adsorptions. The higher valence cations would occupy more active adsorption sites, which was important for the adsorption of positively charged $MB^+$ ions. In addition, it has been proved that ions with a smaller radius could be adsorbed more easily than those with a larger radius.[30] Among these metal cations, $Al^{3+}$ possesses the smallest ion radius (0.053 nm)[37] and the most severe inhabitation for MB adsorption. That is because the smaller radius cations are more competitive with $MB^+$ ions for the available adsorption sites.

*2.4.5. Reusability of the PC Adsorbent.* Reuse performance is one of the vital properties for practical adsorbents. The adsorption and desorption runs were carried out five times using the same sample in this work. As shown in Figure 11, the MB adsorption capability decreased slightly with the increase in reused cycles. In addition, there was a linear relationship between the adsorption capability and the reused cycles. The gentle slope of this line means good reusability performance. Therefore, the OS-based PC shows great potential in practical application for dye removal.

*2.4.6. Mechanism Analysis.* The adsorption process of organic compound ions on the surface of a carbonaceous adsorbent is commonly very complicated.[38] According to another related research,[39] it was mainly affected by the following three factors: (1) the high specific surface area and pore size distribution, (2) the $\pi-\pi$ electron donor−acceptor interaction between the aromatic ring of the organic compound and the graphitic structure of the carbonaceous

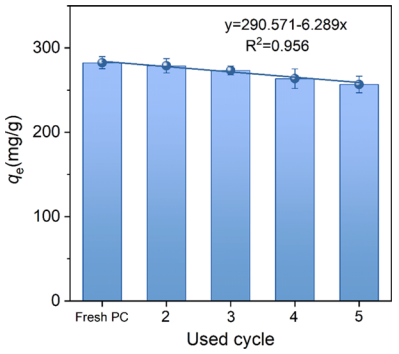


**Figure 11.** Reusability of PC during adsorption−desorption cycles.

material, and (3) the electrostatic interaction or hydrogen bonding effect between the charged ions and surface oxygen-containing functional groups.

The mechanism of MB adsorption onto PC is shown in Figure 12. MB molecules moved into the PC structure through

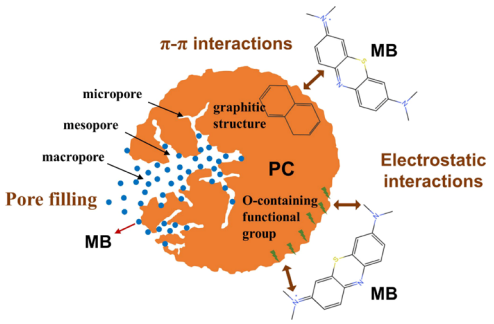


**Figure 12.** Mechanism of the adsorption of MB on PC.

macropores and mesopores and then were adsorbed onto the active sites. An $MB^+$ molecule with a size of about 1.7 nm can be transported and adsorbed in mesopore scales.[40] Therefore, the abundant mesopores in PC structures play a more important role than the specific surface area in MB adsorption, which forms effective pore filling. In addition, electrostatic attraction and hydrogen bonding caused by oxygen-containing functional groups that formed on the surface of PC due to the action of $H_3PO_4$ are also important ways of $MB^+$ adsorption. In addition, the dispersive interaction of $\pi-\pi$ electron stacking would also contribute to the adsorption.

## 3. CONCLUSIONS

In this work, an oily sludge-based PC has been synthesized with $H_3PO_4$ as a catalyst under mild conditions and used as an adsorbent for MB dye removal. RSM has been employed to optimize the synthesis conditions such as the catalytic pyrolysis temperature of 411 °C, the $H_3PO_4$ impregnation ratio of 2.44, and the catalytic pyrolysis time of 59 min. The optimal PC sample possesses a favorable porous structure for adsorption application. The adsorption capacity of MB can reach 322.89 mg/g. The adsorption isotherm, kinetic, and thermodynamic results reveal that MB adsorption on PC is a monolayer adsorption process that is endothermic and spontaneous by the interaction of physical adsorption and chemical adsorption. The adsorption capacity was inhibited by the coexisting metal cations in the background solution due to the competitive adsorption. The higher valence and smaller radius cations show stronger competitive adsorption effects. The MB adsorption


https://doi.org/10.1021/acsomega.1c02575
ACS Omega 2021, 6, 20549−20559

mechanism of PC includes pore filling, $\pi-\pi$ interactions, and electrostatic interaction. Moreover, PC exhibits excellent reusability for adsorption. Therefore, the OS-based PC can be considered as a prospective and economical adsorbent material for practical application. This work reveals a broad prospect for the sustainable utilization of oily sludge wastes.

## 4. EXPERIMENTAL METHODS

**4.1. Materials.** The OS sample was collected from the Shengli petroleum storage depot of Sinopec in Shandong, China. The ultimate analysis and proximate analysis listed in Table S1 were conducted according to the Chinese standard GB/T 212-2008. OS samples were dried at 105 °C for 24 h to get rid of the excess moisture before further use. Deionized water was used throughout the entire experiments.

**4.2. Catalytic Pyrolysis Char (PC) Synthesis.** First, the OS sample was annealed at 700 °C for 60 min under a $N_2$ atmosphere, then ground, and impregnated in excess HF (0.1 mol/L) to remove inorganic impurities. Subsequently, the product was rinsed with deionized water until the filtrate became neutral. Finally, an OS-char (SC) was collected after drying at 105 °C for 24 h.

Afterward, SC was impregnated with $H_3PO_4$ (50 wt %) with a preset mass ratio ($H_3PO_4$-SC). Then, the mixture was agitated (180 rpm) on a magnetic stirrer for 12 h before drying at 105 °C for 4 h. Further catalytic pyrolysis of SC was operated in a tubular furnace, which was heated to the preset temperature with a fixed heating rate of 10 °C/min and maintained at this temperature for a period of time under a nitrogen atmosphere. The solid product was washed with deionized water to remove excess $H_3PO_4$ until the pH of the filtrate reached 7. Ultimately, the PC product was obtained after drying at 105 °C.

**4.3. Single-Factor Experiments: Determination of Suitable Ranges for RSM.** Three significant independent variables in catalytic pyrolysis were investigated in this work, including the catalytic pyrolysis temperature, $H_3PO_4$-SC impregnation mass ratio, and pyrolysis time. To determine appropriate ranges of those variables for the RSM experimental design, several single-factor experiments were operated under the following conditions. First, the catalytic pyrolysis temperature varied between 300 and 700 °C, with a fixed mass ratio of 2.5:1 ($H_3PO_4$-SC) and a pyrolysis time of 60 min. Second, $H_3PO_4$-SC impregnation mass ratio changed in the range of 0.5 to 3.0, with a fixed temperature of 400 °C for 60 min. Third, the sample preparation was conducted under a fixed ratio of 2.5:1, with a fixed temperature of 400 °C for a variable pyrolysis time from 10 min to 120 min.

**4.4. Experimental Design by RSM.** A three-factor and three-level BBD was employed to determine the optimum catalysis pyrolysis process statistically, thereby maximizing the MB adsorption capacity by establishing a continuous quadratic surface model. Design-Expert (version 10.0, Stat-Ease) was applied in this work. For statistical estimation, the catalytic pyrolysis temperature ($X_1$), $H_3PO_4$-SC impregnation mass ratio ($X_2$), and catalytic pyrolysis time ($X_3$) were set as independent variables based on the preliminary single-factor experiments, while the MB adsorption value ($Y$) was selected as a response variable.

Seventeen runs of experiments were designed at three levels (high (+1), central (0), and low (−1)). The following second-order polynomial equation was employed to investigate the interaction between the independent and dependent variables.

$$Y = \beta_0 + \sum_{i=1}^{k} \beta_i X_i + \sum_{i=1}^{k} \beta_{ii} X_i^2 + \sum_{i=1}^{k-1} \sum_{i=i+1}^{k} \beta_{ij} X_i X_j$$

where $Y$ is the predicted response, $\beta_0$ is the constant coefficient, $\beta_i$ is the linear coefficient, $\beta_{ii}$ is the squared coefficient, $\beta_{ij}$ is the interaction coefficient, and $k$ is the number of variables. Analysis of variance was used to decide the goodness of fit of the constructed polynomial model.

**4.5. Characterization.** A $N_2$ adsorption−desorption test was carried out at 77 K (ASAP2020M, Micromeritics) to investigate the porosity of samples. The composition and morphology of samples were analyzed by X-ray diffraction (XRD, X'Pert PRO, PANalytical). The morphological features were observed by scanning electron microscopy (SEM, S-4800 Hitachi). The Raman spectrum was obtained by a LabRAM HR800 Raman Spectrometer at a wavelength of 514 nm. X-ray photoelectron spectroscopy (XPS, Thermo Fisher ESCALAB MK II, USA) was performed to determine the composition and the surface elemental conditions of the sample.

**4.6. Adsorption Experiments.** The adsorption isotherm represents the relationship between the adsorbate concentration of the liquid phase and that of the solid phase when the adsorption process reaches equilibrium.[41] The adsorption equilibrium experiments were carried out using three series of conical flasks with 50 mL of MB solution in different concentrations (25−800 mg/L). After 10 mg of PC adsorbent was added into each conical flask, the mixtures were stirred (180 rpm) in a water bath for 24 h at 25, 35, and 45 °C, respectively. Then, the used PC was separated by micropore filters (0.22 $\mu$m) immediately. The equilibrium concentration of the filtrate was tested by UV/vis spectrophotometry (TU-1900, PERSEE) on the wavelength of 665 nm. The adsorption capacity of MB would be obtained by the following equation:

$$q_e = \frac{(c_0 - c_e)V}{m}$$

where $q_e$ (mg/g) is the adsorption capacity at equilibrium, and $c_0$ and $c_e$ (mg/L) are the initial concentration and the concentration at equilibrium of the dye solution, respectively. $V$ (L) is the volume of solution, and $m$ (g) is the adsorbent dosage.

Adsorption kinetic parameters were commonly used to investigate the adsorption rate, which was closely related to contact time.[30] The kinetic study was used to understand the adsorption process and the adsorption mechanism. Expect from the fact that the initial concentration was fixed at 200 mg/L, the kinetic test was approximately the same as the equilibrium experiment. The concentration of each flask was then measured promptly at preset intervals (0.5 to 60 min). Also, the adsorption capacity of MB at each time was calculated by the following equation:

$$q_t = \frac{(c_0 - c_t)V}{m}$$

where $q_t$ (mg/g) is the adsorption capacity at each setting time $t$ (min), and $c_0$ and $c_t$ (mg/L) are the initial concentration and the concentration at the setting time $t$ (min) of the dye solution, respectively.

The adsorption thermodynamic study is helpful to explore the mechanism of adsorption. The standard Gibbs free energy ($\Delta G^0$), standard enthalpy change ($\Delta H^0$), and standard entropy change ($\Delta S^0$), as important thermodynamic parameters, were


https://doi.org/10.1021/acsomega.1c02575
ACS Omega 2021, 6, 20549−20559

mainly studied. The thermodynamic parameters were calculated based on the data from kinetic experiments by the following equations:

$$\Delta G^0 = -RT \ln K^0$$

$$\ln K^0 = -\frac{\Delta H^0}{RT} + \frac{\Delta S^0}{R}$$

where $K^0$ is the thermodynamic equilibrium constant.

Reusability is an important index to evaluate the economic value of adsorbents.[42] The spent PC adsorbent was rinsed with 0.05 M HCl to release the adsorbed MB. The procedure for the adsorption capacity of regenerated PC is the same as the adsorption equilibrium test at 25 °C. To study the effect of coexisting ions in solution on the adsorption of MB, different inorganic salts such as NaCl, KCl, $MgCl_2$, $CaCl_2$, $FeCl_3$, and $AlCl_3$ were added into the MB solution. The metal cation concentrations were controlled at 0.01 M, and the MB concentration was maintained at 200 mg/L of the mixture solution.

## ■ ASSOCIATED CONTENT

### Supporting Information

The Supporting Information is available free of charge at https://pubs.acs.org/doi/10.1021/acsomega.1c02575.

Calculation methods for adsorption isotherm and kinetic parameters (page S2); Table S1: characteristics of the used OS sample (page S4); Table S2: fit summary of the sequential model (page S4); Table S3: ANOVA of the BBD experimental results (page S5); Table S4: statistical analysis for the quadratic model (page S5); Table S5: adsorption isotherm parameters; Table S6: adsorption kinetic parameters (page S6); Table S7: comparison of the MB adsorption capacity of various adsorbents (page S7); Figure S1: XPS analysis of the PC samples (page S8) and references (page S9) (PDF)

## ■ AUTHOR INFORMATION


### Corresponding Authors

**Xiaoyu Li** − *College of Mechanical and Electronic Engineering, Shandong University of Science and Technology, Qingdao 266590, China; College of New Energy, China University of Petroleum (East China), Qingdao 266580, China;* orcid.org/0000-0001-9283-9476; Email: lixy2018@sdust.edu.cn

**Zhenbo Wang** − *College of New Energy, China University of Petroleum (East China), Qingdao 266580, China;* orcid.org/0000-0002-3055-961X; Email: dxl437@sina.com

### Authors

**Dong Han** − *College of Mechanical and Electronic Engineering, Shandong University of Science and Technology, Qingdao 266590, China; College of New Energy, China University of Petroleum (East China), Qingdao 266580, China*

**Zhiqiang Gong** − *State Grid Shandong Electric Power Research Institute, Jinan 250003, China*

**Lanyue Jiang** − *College of Mechanical and Electronic Engineering, Shandong University of Science and Technology, Qingdao 266590, China*

**Peikun Liu** − *College of Mechanical and Electronic Engineering, Shandong University of Science and Technology, Qingdao 266590, China*

Complete contact information is available at: https://pubs.acs.org/10.1021/acsomega.1c02575


### Notes

The authors declare no competing financial interest.

## ■ ACKNOWLEDGMENTS

This work was supported by the Natural Science Foundation of Shandong Province (ZR2019BEE023 and ZR2020QE199) and the Opening Fund of State Key Laboratory of Heavy Oil Processing (SKLOP202003001).

## ■ REFERENCES


(1) Hu, G.; Li, J.; Zeng, G. Recent development in the treatment of oily sludge from petroleum industry: A review. *J. Hazard. Mater.* **2013**, *261*, 470−490.

(2) Taiwo, E. A.; Otolorin, J. A. Oil Recovery from Petroleum Sludge by Solvent Extraction. *Pet. Sci. Technol.* **2009**, *27*, 836−844.

(3) Jin, Y.; Zheng, X.; Chu, X.; Chi, Y.; Yan, J.; Cen, K. Oil Recovery from Oil Sludge through Combined Ultrasound and Thermochemical Cleaning Treatment. *Ind. Eng. Chem. Res.* **2012**, *51*, 9213−9217.

(4) Zhou, L.; Jiang, X.; Liu, J. Characteristics of oily sludge combustion in circulating fluidized beds. *J. Hazard. Mater.* **2009**, *170*, 175−179.

(5) Leonard, S. A.; Stegemann, J. A. Stabilization/solidification of petroleum drill cuttings. *J. Hazard. Mater.* **2010**, *174*, 463−472.

(6) Koolivand, A.; Abtahi, H.; Godini, K.; Saeedi, R.; Rajaei, M. S.; Parhamfar, M.; seifi, H. Biodegradation of oil tank bottom sludge using a new two-phase composting process: kinetics and effect of different bulking agents. *J. Mater. Cycles Waste Manage.* **2019**, *21*, 1280−1290.

(7) Hu, G.; Feng, H.; He, P.; Li, J.; Hewage, K.; Sadiq, R. Comparative life-cycle assessment of traditional and emerging oily sludge treatment approaches. *J. Cleaner Prod.* **2020**, *251*, 119594.

(8) da Silva, L. J.; Alves, F. C.; de França, F. P. A review of the technological solutions for the treatment of oily sludges from petroleum refineries. *Waste Manage. Res.* **2012**, *30*, 1016−1030.

(9) Aguelmous, A.; El Fels, L.; Souabi, S.; Zamama, M.; Hafidi, M. The fate of total petroleum hydrocarbons during oily sludge composting: a critical review. *Rev. Environ. Sci. Bio/Technol.* **2019**, *18*, 473−493.

(10) Lin, B.; Huang, Q.; Yang, Y.; Chi, Y. Preparation of Fe-char catalyst from tank cleaning oily sludge for the catalytic cracking of oily sludge. *J. Anal. Appl. Pyrolysis* **2019**, *139*, 308−318.

(11) Li, X.; Wang, Z.; Guo, L.; Han, D.; Li, B.; Gong, Z. Manganese oxide/hierarchical porous carbon nanocomposite from oily sludge for high-performance asymmetric supercapacitors. *Electrochim. Acta* **2018**, *265*, 71−77.

(12) Das, B.; Mohanty, K. A review on advances in sustainable energy production through various catalytic processes by using catalysts derived from waste red mud. *Renewable Energy* **2019**, *143*, 1791−1811.

(13) Meng, F.; Gong, Z.; Wang, Z.; Fang, P.; Li, X. Study on a nitrogen-doped porous carbon from oil sludge for $CO_2$ adsorption. *Fuel* **2019**, *251*, 562−571.

(14) Gong, Z.; Meng, F.; Wang, Z.; Fang, P.; Li, X.; Liu, L.; Zhang, H. Study on Preparation of an Oil Sludge-Based Carbon Material and Its Adsorption of $CO_2$: Effect of the Blending Ratio of Oil Sludge Pyrolysis Char to KOH and Urea. *Energy Fuels* **2019**, *33*, 10056−10065.

(15) Li, X.; Liu, K.; Liu, Z.; Wang, Z.; Li, B.; Zhang, D. Hierarchical porous carbon from hazardous waste oily sludge for all-solid-state flexible supercapacitor. *Electrochim. Acta* **2017**, *240*, 43−52.

(16) Gong, Z.; Liu, C.; Wang, M.; Wang, Z.; Li, X. Experimental study on catalytic pyrolysis of oil sludge under mild temperature. *Sci. Total Environ.* **2020**, *708*, 135039.
(17) Del Bubba, M.; Anichini, B.; Bakari, Z.; Bruzzoniti, M. C.; Camisa, R.; Caprini, C.; Checchini, L.; Fibbi, D.; El Ghadraoui, A.; Liguori, F.; Orlandini, S. Physicochemical properties and sorption capacities of sawdust-based biochars and commercial activated carbons towards ethoxylated alkylphenols and their phenolic metabolites in effluent wastewater from a textile district. *Sci. Total Environ.* **2020**, *708*, 135217.
(18) Tian, Y.; Li, J.; Whitcombe, T. W.; McGill, W. B.; Thring, R. Application of oily sludge-derived char for lead and cadmium removal from aqueous solution. *Chem. Eng. J.* **2020**, *384*, 123386.
(19) Mojoudi, N.; Mirghaffari, N.; Soleimani, M.; Shariatmadari, H.; Belver, C.; Bedia, J. Phenol adsorption on high microporous activated carbons prepared from oily sludge: equilibrium, kinetic and thermodynamic studies. *Sci. Rep.* **2019**, *9*, 19352.
(20) Yang, H.; Shen, K.; Fu, P.; Zhang, G. Preparation of a novel carbonaceous material for Cr(VI) removal in aqueous solution using oily sludge of tank bottom as a raw material. *J. Environ. Chem. Eng.* **2019**, *7*, 102898.
(21) Yang, H.; Li, Z.; Fu, P.; Zhang, G. Cr(VI) removal from a synthetic solution using a novel carbonaceous material prepared from oily sludge of tank bottom. *Environ. Pollut.* **2019**, *249*, 843−850.
(22) Mojoudi, N.; Soleimani, M.; Mirghaffari, N.; Belver, C.; Bedia, J. Removal of phenol and phosphate from aqueous solutions using activated carbons prepared from oily sludge through physical and chemical activation. *Water Sci. Technol.* **2019**, *80*, 575−586.
(23) Wang, J.; Sun, C.; Lin, B.-C.; Huang, Q.-X.; Ma, Z.-Y.; Chi, Y.; Yan, J.-H. Micro- and mesoporous-enriched carbon materials prepared from a mixture of petroleum-derived oily sludge and biomass. *Fuel Process. Technol.* **2018**, *171*, 140−147.
(24) Wang, A.-Y.; Sun, K.; Wu, L.; Wu, P.; Zeng, W.; Tian, Z.; Huang, Q.-X. Co-carbonization of biomass and oily sludge to prepare sulfamethoxazole super-adsorbent materials. *Sci. Total Environ.* **2020**, *698*, 134238.
(25) Tian, Y.; Li, J.; Yan, X.; Whitcombe, T.; Thring, R. Co-pyrolysis of metal contaminated oily waste for oil recovery and heavy metal immobilization. *J. Hazard. Mater.* **2019**, *373*, 1−10.
(26) Qu, Y.; Qin, L.; Liu, X.; Yang, Y. Reasonable design and sifting of microporous carbon nanosphere-based surface molecularly imprinted polymer for selective removal of phenol from wastewater. *Chemosphere* **2020**, *251*, 126376.
(27) Hiew, B. Y. Z.; Lee, L. Y.; Lai, K. C.; Gan, S.; Thangalazhy-Gopakumar, S.; Pan, G.-T.; Yang, T. C.-K. Adsorptive decontamination of diclofenac by three-dimensional graphene-based adsorbent: Response surface methodology, adsorption equilibrium, kinetic and thermodynamic studies. *Environ. Res.* **2019**, *168*, 241−253.
(28) Salari, M.; Dehghani, M. H.; Azari, A.; Motevalli, M. D.; Shabanloo, A.; Ali, I. High performance removal of phenol from aqueous solution by magnetic chitosan based on response surface methodology and genetic algorithm. *J. Mol. Liq.* **2019**, *285*, 146−157.
(29) Saleh, T. A.; Adio, S. O.; Asif, M.; Dafalla, H. Statistical analysis of phenols adsorption on diethylenetriamine-modified activated carbon. *J. Cleaner Prod.* **2018**, *182*, 960−968.
(30) Liu, Y.; Li, J.; Wu, L.; Shi, Y.; He, Q.; Chen, J.; Wan, D. Magnetic spent bleaching earth carbon (Mag-SBE@C) for efficient adsorption of tetracycline hydrochloride: Response surface methodology for optimization and mechanism of action. *Sci. Total Environ.* **2020**, *722*, 137817.
(31) Liu, F.; Wang, Z.; Zhang, H.; Jin, L.; Chu, X.; Gu, B.; Huang, H.; Yang, W. Nitrogen, oxygen and sulfur co-doped hierarchical porous carbons toward high-performance supercapacitors by direct pyrolysis of kraft lignin. *Carbon* **2019**, *149*, 105−116.
(32) Ratso, S.; Kruusenberg, I.; Vikkisk, M.; Joost, U.; Shulga, E.; Kink, I.; Kallio, T.; Tammeveski, K. Highly active nitrogen-doped few-layer graphene/carbon nanotube composite electrocatalyst for oxygen reduction reaction in alkaline media. *Carbon* **2014**, *73*, 361−370.
(33) Karnan, M.; Subramani, K.; Srividhya, P. K.; Sathish, M. Electrochemical Studies on Corncob Derived Activated Porous Carbon for Supercapacitors Application in Aqueous and Non-aqueous Electrolytes. *Electrochim. Acta* **2017**, *228*, 586−596.
(34) Chinh, V. D.; Hung, L. X.; Di Palma, L.; Hanh, V. T. H.; Vilardi, G. Effect of Carbon Nanotubes and Carbon Nanotubes/Gold Nanoparticles Composite on the Photocatalytic Activity of TiO2 and $TiO_2$-$SiO_2$. *Chem. Eng. Technol.* **2019**, *42*, 308−315.
(35) Li, X.; Han, D.; Zhang, M.; Li, B.; Wang, Z.; Gong, Z.; Liu, P.; Zhang, Y.; Yang, X. Removal of toxic dyes from aqueous solution using new activated carbon materials developed from oil sludge waste. *Colloids Surf., A* **2019**, *578*, 123505.
(36) Du, M.; Li, J.; Wang, F.; Li, X.; Yu, T.; Qu, C. The sludge-based adsorbent from oily sludge and sawdust: preparation and optimization. *Environ. Technol.* **2020**, 1.
(37) Kilislioglu, A. The effect of various cations and pH on the adsorption of U(VI) on Amberlite IR-118H resin. *Appl. Radiat. Isot.* **2003**, *58*, 713−717.
(38) Li, S.; Huang, L.; Zhang, H.; Huang, Z.; Jia, Q.; Zhang, S. Adsorption mechanism of methylene blue on oxygen-containing functional groups modified graphitic carbon spheres: Experiment and DFT study. *Appl. Surf. Sci.* **2021**, *540*, 148386.
(39) Li, L.; Wu, M.; Song, C.; Liu, L.; Gong, W.; Ding, Y.; Yao, J. Efficient removal of cationic dyes via activated carbon with ultrahigh specific surface derived from vinasse wastes. *Bioresour. Technol.* **2021**, *322*, 124540.
(40) Zha, Z.; Zhu, W.; Chen, F.; Qian, J.; Liu, X.-Q.; Sun, L.-B.; Wu, Z.; Chen, Z. Facile Synthesis of $Co_3O_4$ Nanoparticle-Functionalized Mesoporous $SiO_2$ for Catalytic Degradation of Methylene Blue from Aqueous Solutions. *Catalysts* **2019**, *9*, 809.
(41) Luo, W.; Ouyang, J.; Antwi, P.; Wu, M.; Huang, Z.; Qin, W. Microwave/ultrasound-assisted modification of montmorillonite by conventional and gemini alkyl quaternary ammonium salts for adsorption of chromate and phenol: Structure-function relationship. *Sci. Total Environ.* **2019**, *655*, 1104−1112.
(42) Li, X.-y.; Han, D.; Xie, J.-f.; Wang, Z.-b.; Gong, Z.-q.; Li, B. Hierarchical porous activated biochar derived from marine macroalgae wastes (*Enteromorpha prolifera*): facile synthesis and its application on Methylene Blue removal. *RSC Adv.* **2018**, *8*, 29237−29247.


https://doi.org/10.1021/acsomega.1c02575
*ACS Omega* 2021, 6, 20549−20559